Mapping intertidal oyster farms using unmanned aerial vehicles (UAV) high-resolution multispectral data

Alejandro Román, Hermansyah Prasyad, Simon Oiry, Bede F R Davies, Guillaume Brunier, Laurent Barillé

Estuarine, Coastal and Shelf Science 291 (2023) 108432

Contents lists available at ScienceDirect

Estuarine, Coastal and Shelf Science

journal homepage: www.elsevier.com/locate/ecss

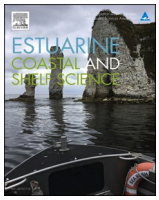

Mapping intertidal oyster farms using unmanned aerial vehicles (UAV) high-resolution multispectral data

Alejandro Román [a,*], Hermansyah Prasyad [b,c], Simon Oiry [b], Bede F.R. Davies [b], Guillaume Brunier [d], Laurent Barillé [b]

[a] Institute of Marine Sciences of Andalusia (ICMAN), Spanish National Research Council (CSIC), Department of Ecology and Coastal Management, Puerto Real, 11519, Spain
[b] Nantes Université, Institut des Substances et Organismes de la Mer, ISOMer, UR 2160, F-44000, Nantes, France
[c] Research and Development Center for Marine, Coast, And Small Island, Hasanuddin University, Makassar, 90245, Indonesia
[d] BRGM French Geological Survey, Cayenne, 97300, French Guiana, France

ARTICLE INFO

Keywords:
Shellfish aquaculture
Unmanned aerial vehicles
Oyster tables
Pacific oyster
Remote sensing

ABSTRACT

In France, oyster aquaculture has been historically developed in intertidal zones, with shellfish farming areas covering much of the Atlantic coast. Monitoring these off-bottom cultures where oysters are grown in plastic mesh-bags set on trestle tables is mandatory for the maritime administration to check compliance with a Structural Plan Document (SPD), while also being important for stock assessment in relation to carrying capacity issues. However, traditional monitoring methods are time-consuming, labor-intensive, and inefficient in covering large intertidal areas. In this study, we used a new GIS-based analytical method to assess the potential of high-resolution Unmanned Aerial Vehicle (UAV) multispectral data to retrieve spatial information on oyster-farming structures using Bourgneuf Bay (France) as a case-study. A non-parametric machine learning algorithm was applied to four UAV flight orthomosaics collected at different altitudes (12, 30, 50, and 120 m) to identify oyster mesh-bags. These supervised classifications achieved overall accuracies above 95% for all tested altitudes. In addition, an accurate distinction of oyster-bag mesh sizes (4, 9 and 14 mm) was obtained for 12–50 m flights, but there was a lower accuracy at 120 m. Across all flights, the 4 mm mesh size was the least well detected (72.14% Producer Accuracy). This information can be used to identify bags with specific mesh-sizes used for spat or adult grow out. Finally, we accurately measured oyster table heights using a high-resolution Digital Surface Model (DSM) derived from Structure from Motion (SfM) photogrammetry. The 50 m flight was suggested as the best compromise to obtain precise measurements of the oyster table heights while covering larger areas than lower altitude flights. This demonstrates that UAV technology can provide a set of spatial variables relevant for shellfish farmers and coastal managers in an efficient, rapid, and non-destructive way to monitor the extent and characteristics of oyster-farming areas regularly.

1. Introduction

The Pacific cupped oyster (*Crassostrea gigas* Thunberg, 1793) is one of the world's most important shellfish mariculture species and is even considered the most cosmopolitan of all oyster species (Harris, 2008). In 2022 it dominated the global shellfish aquaculture production with a total worldwide production of 610300 tonnes (FAO, 2022). It was first introduced to replace depleted stocks of indigenous oysters in several countries, but now this species is the choice oyster of cultivation in many regions of the world (FAO, 2011) and has been successfully cultivated in more than 17 countries (Harris, 2008). Successful production of *C. gigas* is greatly influenced by its ability to adapt to varied environmental conditions by being extremely tolerant to a wide range of seawater temperatures and salinity, resistant to highly turbid areas, able to grow in various latitudes, and exhibiting fast growth (Martínez-García et al., 2021; Miossec et al., 2009).

Since its introduction between 1966 and 1970 (Buestel et al., 2009), *C. gigas* has been successfully cultivated and is the main shellfish culture

* Corresponding author.
E-mail addresses: a.roman@csic.es (A. Román), prasyad@gmail.com (H. Prasyad), simon.oiry@univ-nantes.fr (S. Oiry), bede.davies@univ-nantes.fr (B.F.R. Davies), guillaume_brunier@hotmail.fr (G. Brunier), Laurent.Barille@univ-nantes.fr (L. Barillé).

https://doi.org/10.1016/j.ecss.2023.108432
Received 6 February 2023; Received in revised form 1 July 2023; Accepted 10 July 2023
Available online 11 July 2023

species in France. *C. gigas* production in France topped 79500 tonnes in 2020 (FAO, 2023), making it the biggest oyster producer in Europe. Since the 19th century, oyster culture was established in the intertidal zone with shellfish farms occupying large intertidal areas in the French Atlantic coast (Barillé et al., 2020; Buestel et al., 2009; Palmer et al., 2020). Off-bottom culture is France's most widely used farming technique for oyster cultivation. Oysters are typically grown in plastic mesh bags, suspended on trestle tables at *ca.* 1 m above the substrate, which are exposed during low tides (Barillé et al., 2020; Kervella et al., 2010).

In Europe, individual states typically manage aquaculture activities, each with its own regulatory and management policies. Marine aquaculture in France is regulated by marine fisheries legislation Law No.97-1051 on Maritime Fisheries and Mariculture and Decree of January 9, 1852 on Maritime Fisheries (Hedley and Huntington, 2009). All intertidal areas in France belong to the Public Maritime Domain under the supervision of the State Directorate of Maritime Affairs (Barillé et al., 2020), using a concession system to grant state-owned intertidal areas for shellfish farming. Oyster concessions are usually leased for 30 years and must comply with several technical specifications such as the type of culture and the rearing density (Barillé et al., 2020). The shellfish farmers have to deal with the numerous technical requirements outlined in a Structural Plan Document (SPD) (Barillé et al., 2020) to develop their practices over a large portion of the French intertidal area. As a result, this becomes a time-consuming and labor-intensive task for the Maritime Affairs, involving regular monitoring of the extent and status of the oyster farms, verification of compliance with marine spatial plans or regulations, and determining whether it is adversely affecting the environment (Bell et al., 2020; Buestel et al., 2009). Oyster table height is one of the variables monitored by the administration. It is crucial for intertidal oyster farming, being related to growth and mortality caused by herpesvirus 1 (OsHV-1 µVar) (Lorgeril et al., 2018). Until now, table heights have been assessed manually, but could greatly benefit from an automated remote sensing method.

The development, practice and management of the fishery/aquaculture industry can be supported by satellite remote sensing technology, which offers a unique capability to obtain valuable data at different spatial and temporal scales and resolutions (Gernez et al., 2021; Ouellette and Getinet, 2016). In addition, regular and repeated satellite observations can be useful for site selection, production monitoring, water quality monitoring, or to inspect the environmental impacts of oyster-farming areas (*e.g.* Gernez et al., 2014, 2017; Jiang et al., 2022; Palmer et al., 2020). However, some gaps in satellite imagery constrain its use, such as cloud coverage, the need for atmospheric corrections, or the asynchronism with tides (Chand and Bollard, 2021). Furthermore, satellite imagery at coarse spatial resolution can potentially confuse machine learning techniques especially when assessing complex and heterogeneous environments (Ouellette and Getinet, 2016; Windle et al., 2022).

In recent years, UAVs have emerged as a promising tool to collect high-resolution data of coastal and intertidal areas, offering new opportunities for precise farm management (Candiago et al., 2015; Windle et al., 2019, 2022). In fact, they offer a low-cost, rapid, repeatable and time-efficient alternative that does not carry the main limitations of satellite remote sensing (Espriella et al., 2020; Román et al., 2021; Windle et al., 2019, 2022). Pixel-based classification methods have been used to distinguish different features and objects in marine environments using remote sensing imagery (Joyce et al., 2018), since they show distinctive spectral signatures that can be used to classify them adequately. In addition, several studies showed that oysters have higher reflectance in the NIR wavelength region due to the surface reflection from the shell (Chand and Bollard, 2021; Le Bris et al., 2016). Consequently, research concerning the use of UAVs for oyster mapping has been nearly exclusively focused on the characterization of oyster reefs (*e.g.* Chand and Bollard, 2021; Espriella and Lecours, 2022; Espriella et al., 2020; Windle et al., 2019, 2022), while their potential for monitoring cultivated oyster in farming areas has yet to be tested to the best of our knowledge.

In this study, we assessed the potential of high-resolution data collected by a UAV-mounted multispectral camera to identify oyster tables occupied with oyster mesh-bags in a case study on the French Atlantic coast (Bourgneuf Bay). Several flights at different altitudes were carried out in order to determine the best Ground Sampling Distance (GSD) to first detect the oyster tables, and second to identify the different oyster-bag mesh sizes. A machine learning classification algorithm was applied to obtain thematic maps of oyster concessions, validated with *in situ* data taken during the field survey. Finally, oyster table height was estimated using a high-resolution Digital Surface Model (DSM) obtained with Structure from Motion (SfM) photogrammetry. This was also validated with *in situ* field data.

2. Materials and methods

2.1. Study area

Bourgneuf Bay is a macrotidal bay located southeast of the Loire estuary on the French Atlantic coast (Fig. 1A), with a tidal amplitude between 2 and 6 m (Le Bris et al., 2016). The intertidal area is mostly composed of large mudflats and rocky areas, and it is mainly used for shellfish aquaculture (Gernez et al., 2017; Le Bris et al., 2016). The pacific oyster *Crassostrea gigas* (Thunberg) is extensively cultivated in this bay, with 5330 metric tons produced in 2012 on its approximately 283 aquaculture farms, most being small family-run companies (Guillotreau et al., 2018). This study was conducted in the oyster-farming area of "La Bernerie" (Fig. 1B–E, 47°03′N, 2°01′W) located in the northern part of the bay. The selection of this area was primarily based on the spectral complexity of the oyster concessions and their surrounding environment, composed of mudflats, wild oyster reefs, and rocky areas colonized by macroalgae. In addition, its accessibility by foot during low tide facilitated the easy movement of the equipment.

2.2. UAV data collection

In this study, a quadcopter DJI Matrix 210 (M210) equipped with the MicaSense RedEdge-MX multispectral dual sensor, which collects spectral information with 10 bands, was used: coastal blue (444 ± 28 nm), blue (475 ± 32 nm), green (531 ± 14 nm and 560 ± 27 nm), red (650 ± 16 nm and 668 ± 14 nm), red Edge (705 ± 10 nm, 717 ± 12 nm and 740 ± 18 nm) and near-infrared (NIR, 842 ± 57 nm). The multispectral sensor controls light conditions and solar angle changes during the flight by using its own Downwelling Light Sensor (DLS) with built-in GPS. In addition, the included calibration panel (RP05-2025214-OB), which was photographed moments before each UAV flight, was used to perform radiometric calibration. This process enables the conversion of raw pixel values captured by the multispectral sensor into reflectance, thus ensuring that the final orthomosaics do not appear underexposed, exhibit irregular coloration, or display extreme banding.

Data collection was conducted on the October 12, 2022, during low tide and clear sky meteorological conditions. A total of four flights at different altitudes (12, 30, 50, and 120 m above the ground) were performed in order to elaborate high-resolution reflectance orthomosaics for each spectral band and DSM. Flight planning was carried out with the DJI Pilot (Dà-Jiāng Innovations (DJI), Shenzen, Guangdong, v. 1.1.5) application and then uploaded to the UAV computer system. Flight parameters considered a 70–80% front and side overlap and were maintained uniformly along the entire study area due to the MicaSense's own terrain following tool. In addition, the battery autonomy limited the duration of the flights to no more than 30 min, although the flight at 120 m high was completed in two segments. French and European civil aviation regulations were followed during all UAV operations.

The software Pix4D mapper v.1.8.3 (Pix4D SA, Lausanne, Switzerland) was used to produce reflectance orthomosaics and topographic products for each UAV flight using a SfM photogrammetric

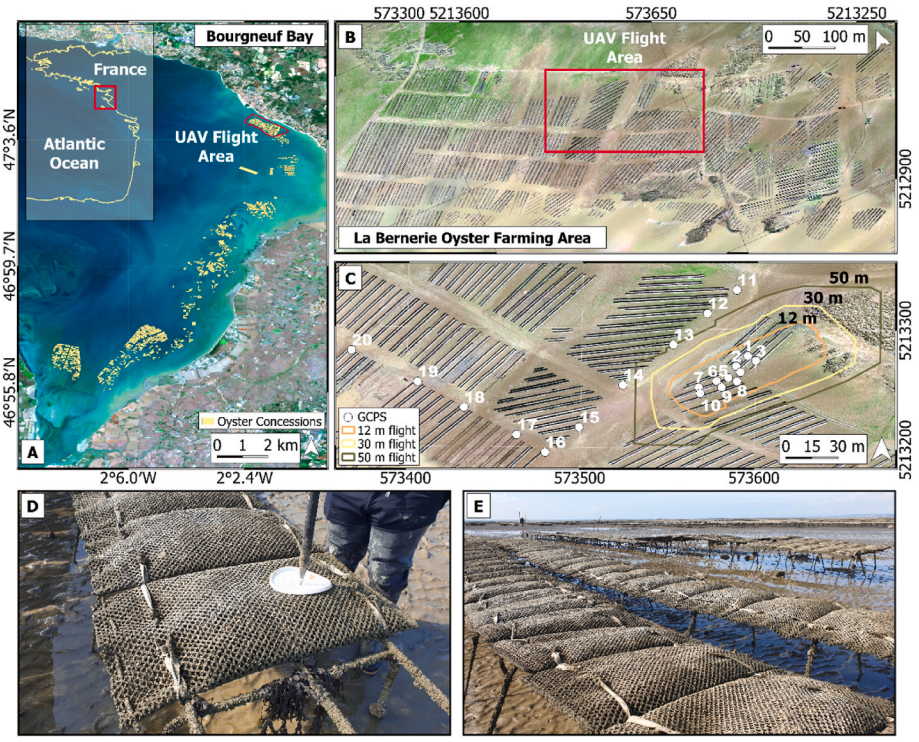

Fig. 1. A) Sentinel-2 true color composite (September 20, 2022) of the study area location of Bourgneuf Bay (French Atlantic coast). Framed in yellow are the oyster concessions according to the shellfish farming cadaster. **B)** Oyster-farming area of "La Bernerie", showing oyster concessions organized in parallel lines of oyster trestle table. **C)** Detail of the UAV flight area showing the shapes of the different altitude flights performed and the 20 GCPs used for precise geolocation. **D)** Oyster table height measurement with a dGPS for validation. **E)** Oyster mesh-bags set on parallel rows of trestle tables. Coordinate reference system for panel A: WGS84, and for panels B–C: WGS84/UTM Zone 30N. (For interpretation of the references to color in this figure legend, the reader is referred to the Web version of this article.)

technique. After importing the selected images, a sparse point cloud was reconstructed by "capture alignment". A 3D dense point cloud, an interpolated DSM and a Digital Terrain Model (DTM) were generated before the mosaicking process. In the last processing step, the radiometric calibration "Sun Irradiance and Sun Angle" was followed to convert radiance into reflectance since the meteorological conditions did not change during the performance of the UAV flights. The resulting orthomosaics were projected to RGF93 Lambert 93, EGM 2008. The GSD achieved for each orthomosaic and for the corresponding generated DSM and DTM are displayed in Table 1.

2.3. Ground reference data

Ground Control Points (GCPs) were uniformly scattered along the study area for georeferencing UAV imagery (Fig. 1C). However, due to the significantly larger coverage area of the 120 m flight, it was not feasible to achieve full coverage distribution with GCPs. Measurements at those discernible white georeferenced targets were collected prior to each flight using a Trimble © Geo XH 6000 differential GPS (dGPS), with a horizontal and vertical accuracy of 0.1 m. After "capture alignment" with Pix4D mapper software, the GCP information was imported using the GCP/MTP Manager and marked using the 3D dense point cloud, obtaining a mean Root Mean Square (RMS) error in georeferencing of 0.145 cm (12 m flight), 0.926 cm (30 m flight), 0.15 cm (50 m flight) and 1.105 cm (120 m flight). Similarly, 46 *in situ* table height points were measured above and under the oyster tables, to evaluate the accuracy of the predicted table heights retrieved from the SfM photogrammetry. In addition, more than 50 ground-based photographs and measurements of the oyster-bag mesh sizes were carried out to validate the bag mesh-size classification accuracy.

Table 1
GSD obtained on each UAV reflectance orthomosaic and the corresponding DSM and DTM generated.

Flight Altitude (m)	DSM (cm/px)	DTM (cm/px)	Reflectance orthomosaics (cm/px)
12	0.83	4.13	0.83
30	2.17	10.85	2.17
50	3.56	17.80	3.56
120	8.44	42.20	8.44

2.4. Data analysis

Fig. 2 summarizes the workflow followed in this study to achieve the proposed objectives. Firstly, the oyster tables were detected and classified from the UAV reflectance orthomosaics generated for each flight altitude using a non-parametric machine learning technique (Support Vector Machine, SVM algorithm) for supervised classification. Secondly, the same technique was applied to all the flight altitudes in order to distinguish the different oyster bag mesh-sizes. Finally, oyster table height was estimated as the difference between the DSM and DTM after SfM photogrammetry processing.

2.4.1. Oyster tables and oyster-bag mesh size detection

This study used Support Vector Machine (SVM) to identify and map oyster tables using pixel-based classification. SVM was selected since it can handle statistically unknown large datasets, applying kernel functions to map them into a larger-dimensional space where a hyperplane aims to correctly divide different classification classes (Bahari et al., 2014; Vapnick, 1995). Miranda et al. (2020) suggested that running the SVM algorithm with the radial basis function set as a kernel parameter offers the best outcomes when working with optically complex systems such as this case study in intertidal areas. The SAGA GIS software (Conrad et al., 2015) was used to perform SVM classification, by using all bands as inputs when performing image classification at each flight altitude.

For oyster tables detection, 50 training polygons of a maximum size of 1 m^2 were manually created for each class and distributed throughout the entire orthomosaics. Up to five different classes were selected and repeated in all flight altitudes tested (12, 30, 50, and 120 m): "oyster tables", "water", "muddy substrate", "shadows", and "microphytobenthos (MPB)". The selection of a constant quantity for all UAV surveys was based on achieving optimal classification accuracies while maintaining efficient processing capacities. Regarding oyster-bag mesh

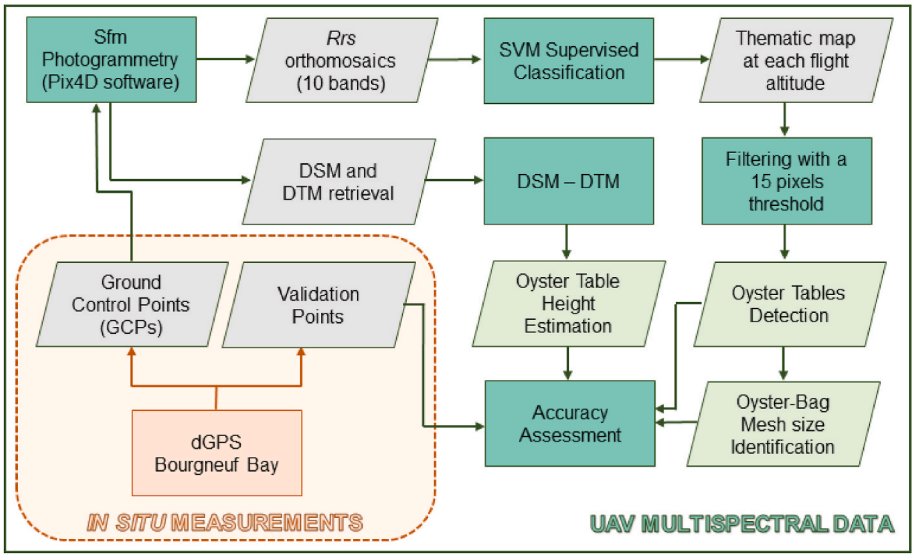

Fig. 2. Schematic representation of the workflow. SfM photogrammetry is applied to UAV multispectral data to generate reflectance orthomosaics and topographic models (DSM and DTM). SVM classifier is applied to reflectance orthomosaics for oyster tables and oyster-bag mesh size detection. Oyster table height is calculated as the difference between the DSM and the DTM. Results are validated with an accuracy assessment based on Oloffson et al. (2014) for supervised classification and accuracy statistics calculated from ground reference data measured with a dGPS.

size detection, five different classes were chosen for all altitudes tested, which provided the highest spatial resolution: "4 mm mesh size", "9 mm mesh size", "14 mm mesh size", "shadows", and "other". Unlike oyster table detection, the number of training polygons does not remain constant because there is greater spectral homogeneity between the selected classes, requiring more trial and error to achieve a satisfactory result. Finally, the obtained classification results were imported into the QGIS software (QGIS Development Team, Geographic Information System, Open Source Geospatial Foundation Project, v.3.16.14, https://qgis.org) to filter them through sieving groups of 15 pixels (or fewer) that corresponded with misclassification errors (associated with noise or unwanted classifications). These pixels were reclassified by considering the value of the most dominant category in their neighborhood.

An accuracy assessment of each SVM classification was performed following Oloffson et al. (2014). Reported classes were compared with randomly selected points (different from training polygons) that were manually classified to generate a confusion matrix that describes the classification model's performance. Some statistical parameters are included in the confusion matrix such as (i) Overall Accuracy (OA), which defines the number of correctly classified pixels from the total sample size, with values above 80% considered as good and reliable (Alberg et al., 2004; Kay et al., 2017; Oloffson et al., 2014); (ii) Kappa coefficient, that measures the relationship between classification and ground truth values, and for which values closer to 1 are considered as better results; (iii) user's accuracy, that indicates the probability that a predicted classification value is correctly classified; and (iv) producer's accuracy, that indicates the probability that a given classification value is correctly classified. User accuracy focuses on the model's ability to avoid false negatives, while producer accuracy emphasizes the model's ability to avoid false positives (Román et al., 2021).

2.4.2. Oyster table height estimation

In this study, we evaluated the most suitable flight height to obtain precise measurements of the oyster table heights, for which all the DSM and DTM retrieved from photogrammetry with Pix4D mapper were used (Table 1). Oyster table heights were estimated by subtracting the DTM from the DSM. The DSM constitutes a relief that includes all the surface elements, such as the oyster tables, the wild oyster reefs, rocky areas, or other elements present in the study area. The DTM shows just the bare substrate surface, so the difference between both models would describe the oyster table heights (Mallet and David, 2016). To assess the accuracy of oyster table height modelled from photogrammetric products, these modelled oyster table heights were assessed as function of *in situ* oyster table heights (continuous) and UAV flight altitudes (categorical: 12 m, 30 m, 50 m and 120 m) using linear regression within the programming language R (Equation (1) derived from with the "equatiomatic" package: Anderson et al., 2023, R Core Team, 2022). Linear regression estimates and 95% confidence intervals were calculated and visualised using the "tidyverse" ecosystem of packages (Wickham, 2022). Sample against fitted residuals, quartile-quartile and autocorrelation of temporally sequential simples were assessed visually, to fit assumptions of the model used.

$$\begin{aligned}\text{Pred} &= \alpha + \beta_1(\text{True}) + \beta_2(\text{Altitude}_{30\text{ m}}) + \\ &\beta_3(\text{Altitude}_{50\text{ m}}) + \beta_4(\text{Altitude}_{120\text{ m}}) + \beta_5(\text{True} \times \text{Altitude}_{30\text{ m}}) + \\ &\beta_6(\text{True} \times \text{Altitude}_{50\text{ m}}) + \beta_7(\text{True} \times \text{Altitude}_{120\text{ m}}) + \varepsilon\end{aligned} \quad \text{(Eq.1)}$$

where "Pred" is the modelled oyster table heights from photogrammetric products and "True" is the *in situ* measured oyster table heights.

3. Results

3.1. Oyster table detection

Reflectance orthomosaics were used to map oyster tables within concessions through the application of the non-parametric machine learning algorithm SVM (Fig. 3). Three examples of classified concessions are presented for a 120 m flight (Fig. 3: B, C and D), where oyster tables footprints were identified above three different backgrounds: water, MPB, and mud. Using VNIR (visible and near-infrared) imagery, it was possible to accurately map not only the oyster table footprint but also the type of background surrounding the tables. For the 120 m flight, the OA of the classification was 97.47% irrespective of the type of background (Table 2). In addition, oyster tables represented 2.19 ha (17.38% of the concession's surface; Fig. 3) in the selected 12.6 ha of oyster concessions analysed.

Performance was evaluated by varying the UAV flight altitude over *ca.* 2000 m^2 area common to all flights (see Fig. 1C), so that the best parameters for oyster table detection could be determined when planning UAV flights. SVM classification of reflectance orthomosaics was obtained at different flight altitudes: 12, 30, 50, and 120 m (Fig. 4). Visual examination of the resulting thematic classifications indicated that the technique performed well at each altitude. Supporting the aforementioned statement, OA above 97% and Kappa coefficient of above 0.93 were obtained for each flight in the SVM accuracy assessment (Table 2). The user and producer accuracies also showed values

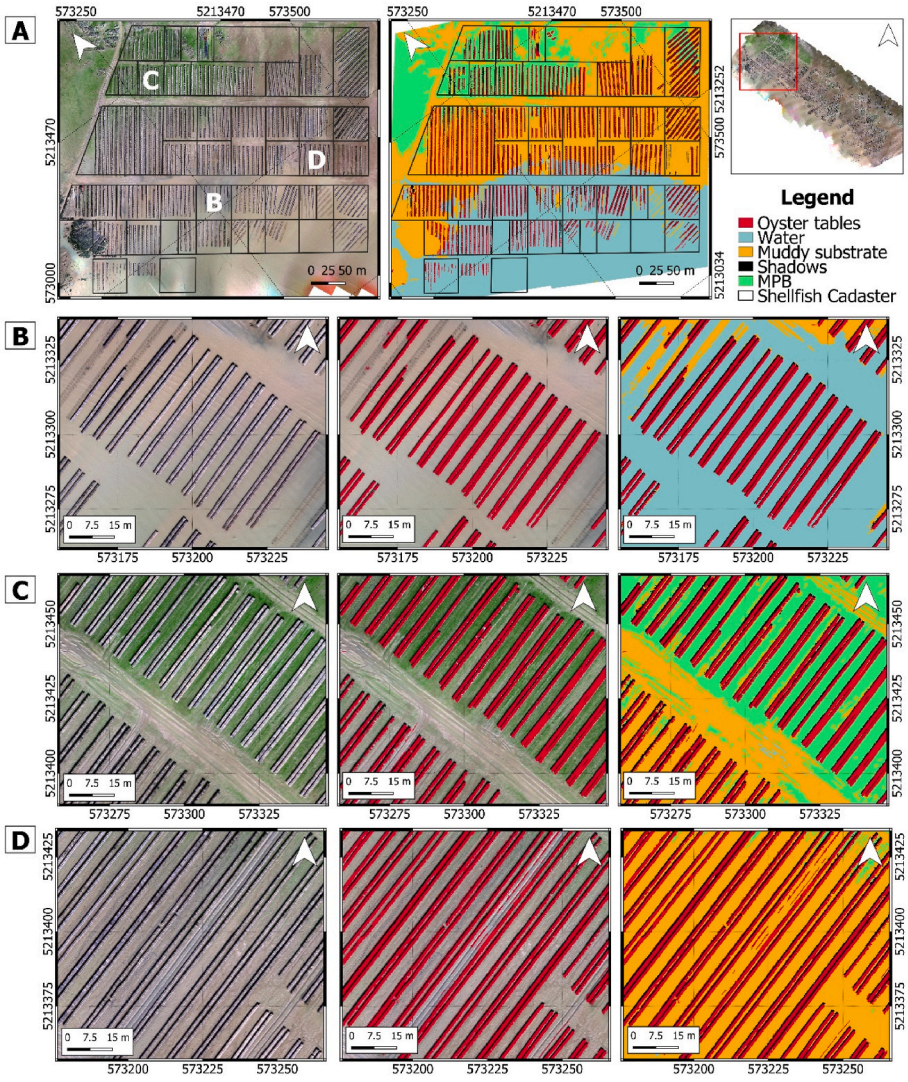

Fig. 3. A) Selected area of oyster concessions at "La Bernerie" (France) oyster-farming site. SVM classification for identifying oyster table footprint over the three different backgrounds (water, MPB, and mud) in the 120 m UAV flight. Three examples of oyster concessions are represented with: **B)** a water layer; **C)** dense MPB biofilms colonizing the substrates; and **D)** bare muddy substrate. The first column is an RGB composite from red-668 nm, green-560 nm, and blue-475 nm UAV multispectral bands. SVM results are shown in second (just oyster tables) and third (oyster tables and backgrounds) columns. (For interpretation of the references to color in this figure legend, the reader is referred to the Web version of this article.)

Table 2
Accuracy assessment of the SVM classification generated from UAV imagery at each flight altitude (12, 30, 50, and 120 m, respectively) using the SVM algorithm, including user accuracy ("U-acc"), producer accuracy ("P-acc"), the OA (%) and the Kappa coefficient.

Class	12 m flight		30 m flight		50 m flight		120 m flight	
	U-acc	P-acc	U-acc	P-acc	U-acc	P-acc	U-acc	P-acc
Oyster Table	91.59	88.19	98.11	97.66	96.18	95.51	94.11	95.32
Other	99.43	99.51	98.25	99.51	98.37	99.61	98.05	99.47
Shadows	98.28	95.93	96.97	86.77	97.39	87.24	97.26	82.82
OA (%)	97.99		98.13		98.00		97.47	
Kappa coefficient	0.95		0.95		0.94		0.93	

above 90% for oyster tables detection, without important disparities with different surrounding backgrounds. In addition, very small differences were found in oyster tables area estimates from a small common area between flights (Fig. 4A), representing approximately 13.52% (255.41 m^2) for the 30 m flight, 13.57% (256.27 m^2) for the 50 m flight and 13.34% (251.93 m^2) for the 120 m flight.

3.2. Oyster-bag mesh size detection

For the highest spatial resolution UAV flight (8.3 mm/px at 12 m), the SVM technique was also applied in order to identify oyster-bag mesh sizes (4, 9, and 14 mm). With this method, it was possible to detect slight spectral differences between the different oyster-bag mesh sizes, due to the presence of epibionts and variable spectral mixture between the mesh and the oysters themselves. Oyster-bag mesh sizes classification compared to *in situ* validation points showed consistent results (Fig. 5 and Table 3: 97.99% and 0.95 for OA and Kappa coefficients, respectively). However, some small disparities were found when discriminating the 4 mm mesh size (Table 3: Producer Accuracy = 72.15%).

The SVM technique was also applied to the rest of the flight heights to analyse the method's performance with decreasing spatial resolution (2.17 cm/px at 30 m; 3.56 cm/px at 50 m; and 8.44 cm/px at 120 m). Validation points indicated consistent results for oyster-bag mesh size detection at these flight altitudes (Fig. 6), with similar OA and Kappa

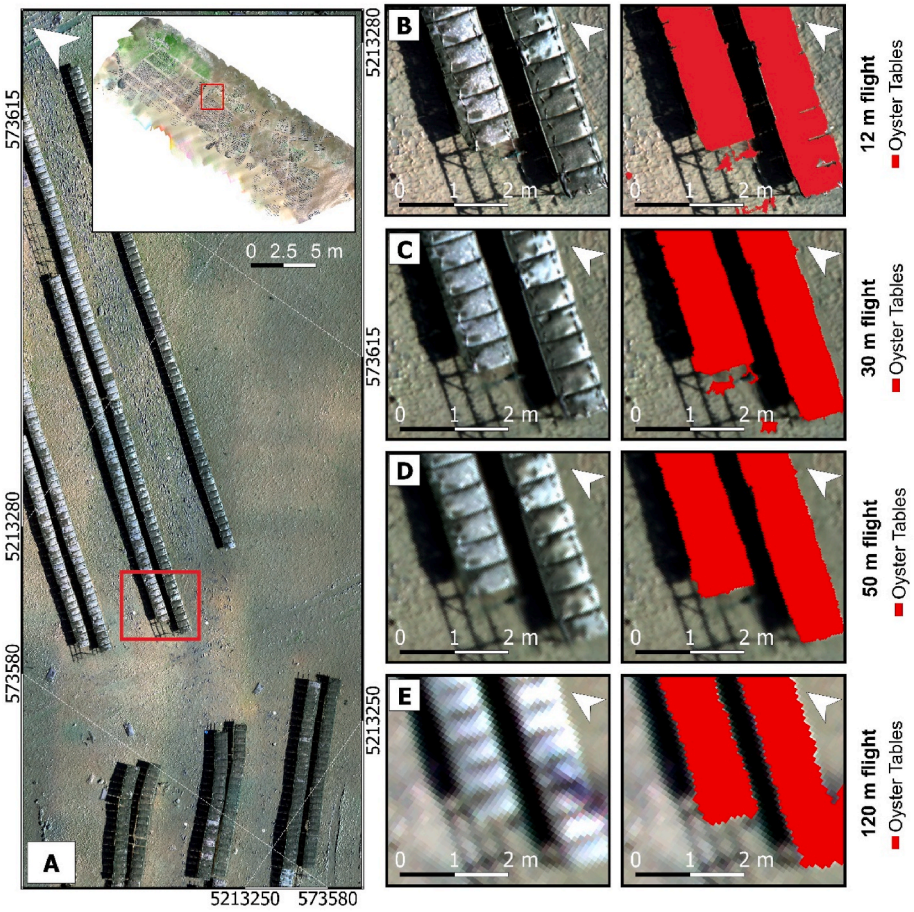

Fig. 4. Oyster table detection at four UAV flight altitudes (12, 30, 50 and 120 m), of **A)** an area selected from the 12 m flight image. Detailed RGB composite and SVM classification at **B)** 12 m, **C)** 30 m, **D)** 50 m, and **E)** 120 m. Note that X and Y coordinates are sometimes listed on the same axis.

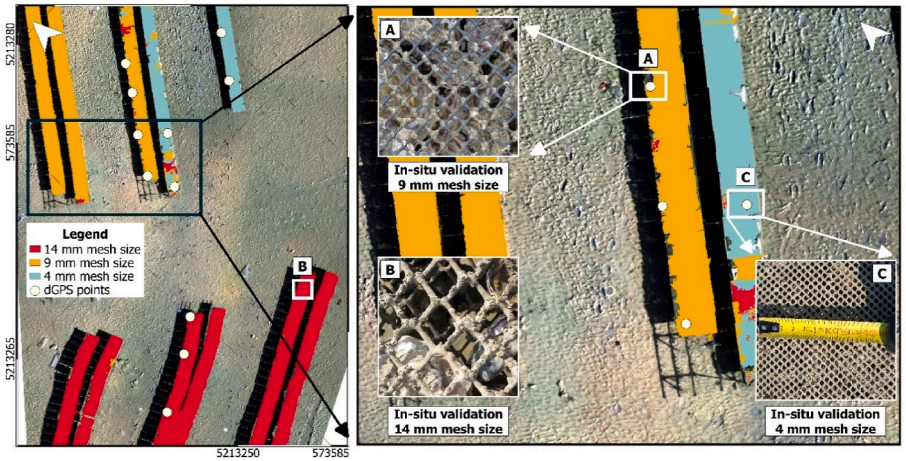

Fig. 5. Oyster-bag mesh sizes detection at a 12 m UAV flight altitude. Examples of *in situ* measurements taken over: **A)** 9 mm; **B)** 14 mm; and **C)** 4 mm mesh sizes. In situ dGPS validation points are represented by white circles.

coefficient values at 30 and 50 m heights (Fig. 6: 95.88% and 94.69% for OA; and 0.91 and 0.90 for Kappa coefficient, respectively). However, an increased number of misclassifications were observed when performing the method at 120 m (Fig. 6: 86.97% and 0.71 for OA and Kappa coefficient, respectively). As with the 12 m flight, confusion matrices of the other flights (see Supplementary Material Section) showed lower producer accuracy values especially when discriminating the 4 mm mesh size from the rest.

3.3. Oyster table height estimation

Oyster table heights were estimated by subtracting the DTM from the DSM, obtaining elevation models for each UAV flight altitude (Fig. 7A). Across all flight altitudes the modelled oyster table heights and the *in situ* table heights showed a significant positive relationship (Table 4 and Fig. 7B). The lowest flight altitudes (12 and 30 m) showed similar patterns of consistently overestimating oyster table heights by ~ 10 cm,

Table 3
Confusion matrix and accuracy assessment of the SVM classification generated from UAV imagery at 12 m for the oyster-bag mesh size detection. Numbers correspond to the polygons of each training classified classes.

Class	Other	14 mm size	4 mm size	9 mm size	Shadows	Total
Other	527	0	2	0	1	530
14 mm size	3	151	4	3	4	165
4 mm size	0	1	117	7	1	126
9 mm size	2	2	8	132	2	146
Shadows	2	1	0	0	171	174
Total	534	155	131	142	179	1141
User Accuracy	99.43	91.52	92.86	90.41	98.28	
Producer Accuracy	99.51	98.24	72.15	94.18	95.92	
Kappa hat	0.98	0.91	0.93	0.90	0.98	
OA (%)						97.99
Kappa coefficient						0.95

while increasing flight altitude caused a consistent underestimation of the table height of ~15 cm for the 120 m flight (Fig. 7B). The middle altitude flight (50 m) showed the least consistent predictions with overestimation at lower *in situ* heights and underestimation at higher *in situ* heights, yet was closest to the *in situ* values in the centre of the values measured (Fig. 7B).

4. Discussion

This research proposes a remote sensing approach for the monitoring of intertidal oyster-farming areas based on very high spatial resolution drone data. A workflow was developed using a UAV-mounted multispectral camera and derived SfM photogrammetric products. Spectral and topographic metrics were tested at different flight altitudes and compared with *in situ* data to determine the best UAV flight settings for shellfish aquaculture areas monitoring. The methodology could be transferable to the Maritime Administration and shellfish farmers' representatives for precision mapping and management at the spatial level of oyster concessions. The limitations and constraints of the proposed method are further discussed.

4.1. Oyster tables detection

The continuous monitoring of coastal aquaculture areas is necessary to deal with carrying capacity issues and associated production loss or environmental impacts if not managed properly (Gernez et al., 2021; Pincinato et al., 2021). In the last few years, different remote sensing products have been used covering variable spatial resolutions, in order to generate spatial tools to support shellfish aquaculture (*e.g.* Barillé et al., 2020; Dean et al., 2013; Gernez et al., 2017; Jiang et al., 2022; Saitoh et al., 2011; Snyder et al., 2017). Moderate spatial resolution sensors such as MODIS or MERIS at 250 m or 300 m, provide useful information for site selection (Palmer et al., 2020) quantifying the spatio-temporal variability of environmental variables such as chlorophyll-a, turbidity, or surface temperature (Barillé et al., 2020), but are too coarse for analysis at the farm level. Higher spatial resolution sensors such as Sentinel-2 are spatially better suited (Gernez et al., 2017), but the lack of flexibility in acquisition is a strong limitation in intertidal zones regarding low tide constraints. Consequently, new approaches that require higher spatial resolution strategies to obtain detailed information at the level of an oyster concession (median area of 3375 m^2 in Bourgneuf Bay) to identify oyster tables and oyster bags mesh size.

The results obtained in this study demonstrated the potential of a UAV with a ten band multispectral sensor as a versatile and flexible solution to accurately detect and map oyster table footprint, through the use of the non-parametric machine learning algorithm SVM. Miranda et al. (2020) suggested that running the SVM algorithm with the radial basis function set as a kernel parameter offers the best outcomes when working with optically complex systems such as this case study in intertidal areas. In this work, SVM performed well regardless of the type of substrate the oyster table was found on. The marked spectral

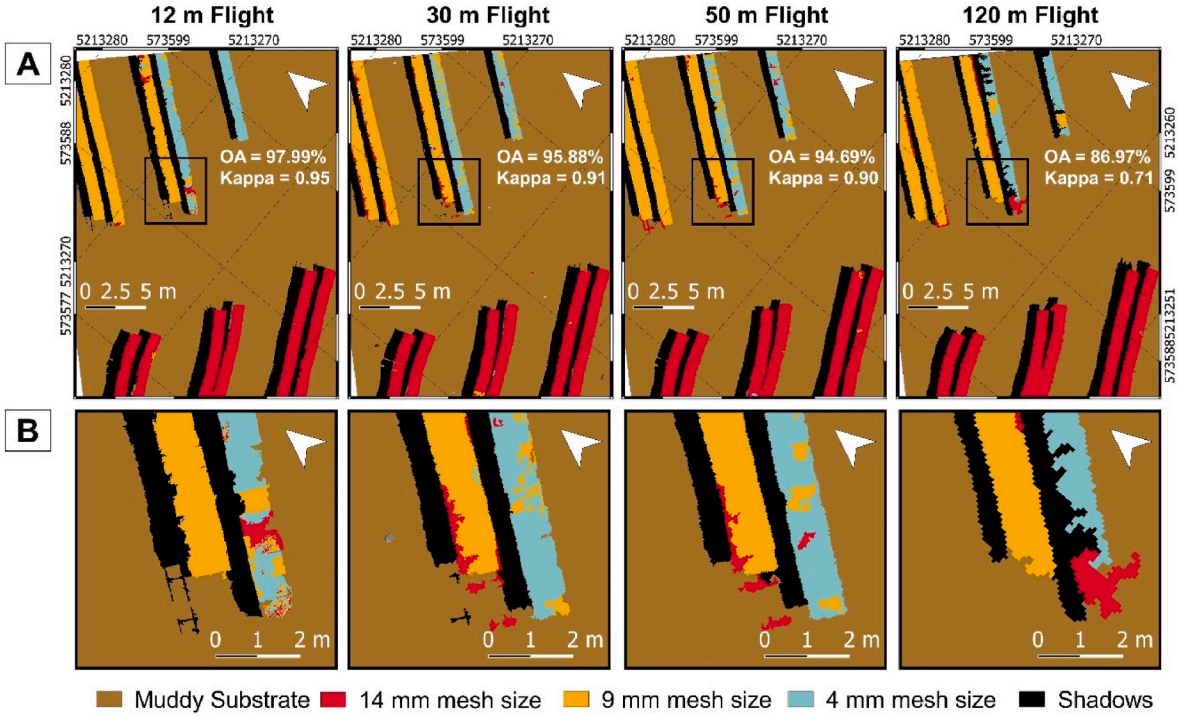

Fig. 6. A) SVM performance for oyster-bag mesh sizes detection at each UAV flight altitude (12, 30, 50, and 120 m, respectively). OA and Kappa coefficient are also displayed in the figure. Black box indicates the area zoomed in B. **B)** Zoomed in area of each classification over a paired row of oyster tables (9 mm and 4 mm mesh size, respectively) at each altitude.

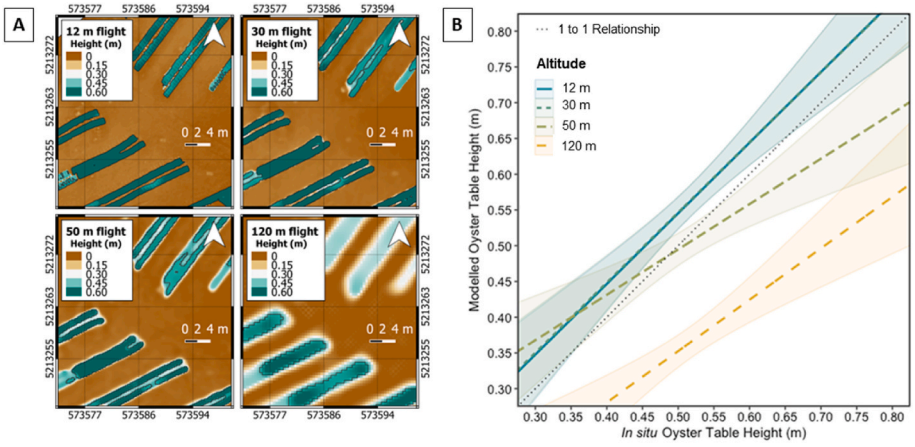

Fig. 7. A) Oyster table height maps (height expressed in meters) retrieved from the DSM and DTM obtained after SfM photogrammetry for each UAV flight (12, 30, 50, and 120 m). **B)** Linear regression modelled oyster table height (m) as a function of *in situ* oyster table height (m) and UAV flight altitude (m) with the ideal 1 to 1 relationship plotted as a dotted black line. Coloured lines show model estimates with 95% confidence intervals displayed by shading. Note 30 m regression line follows, almost identically that of the 12 m line and is barely discernible.

Table 4
Linear regression outputs from modelled oyster table height (m) as a function of *in situ* oyster table height (m) and UAV flight altitude (m). True is used to signify the *in situ* measured oyster table heights. Bold values denote significant p values (<0.05) and asterick's define level of significance: $p < 0.0001$ = "<0.0001***"; $p < 0.001$ = "***"; $p < 0.01$ = "**"; $p < 0.05$ = "*".

Terms	Estimate	Std. Error	t value	p value
(Intercept)	0.051	0.069	0.734	0.470
True	0.988	0.134	7.380	**<0.0001*** **
12–30 m	0.005	0.099	0.047	0.960
12–50 m	0.126	0.099	1.280	0.210
12–120 m	−0.058	0.099	−0.590	0.560
True: 12–30 m	−0.007	0.189	−0.037	0.970
True: 12–50 m	−0.353	0.189	−1.870	0.067
True: 12–120 m	−0.269	0.189	−1.420	0.160

differences between the oyster table covered with mesh bags and the backgrounds allowed an effective delimitation and differentiation from water, MPB and mud. Interestingly, MPB was well classified, which is an advantage of high-resolution VNIR multispectral sensors. Beyond detecting oyster tables, this classification method can be useful for precisely monitoring benthic vegetation. Top-down and bottom-up processes occur between oyster populations and benthic primary producers (Newell, 2004). Oysters can stimulate the growth of benthic diatoms from the MPB (Echappé et al., 2018), but resuspended MPB can represent a significant fraction of an oysters diet (Decottignies et al., 2007). The infrared bands of the multispectral sensor allowed the identification of macroalgae growing on the oyster bags (Fig. 8A–C). This growth of macroalgae was marginally observed in this study but can be very common in spring and summer. Some misclassifications were observed when the SVM had to differentiate between two spectrally similar classes such as wild oyster reefs and oyster tables (Fig. 8D).

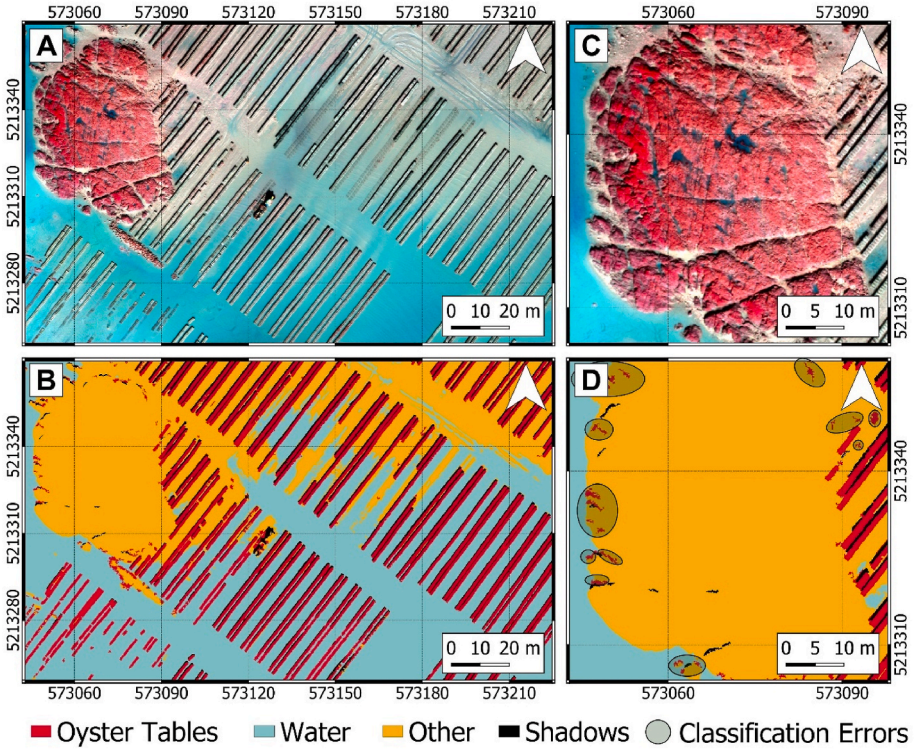

Fig. 8. A) False color composite (NIR 840 nm - red 668 nm – green 560 nm Micasense RedEdge-MX bands) and **B)** SVM classification of the 120 m flight. **C)** Detail of a rocky area where **D)** classification errors are identified with grey ellipses corresponding to wild oyster reefs growing at the vicinity of oyster-farming areas. (For interpretation of the references to color in this figure legend, the reader is referred to the Web version of this article.)

However, this did not impact the oyster table footprint identification as oyster reefs occurred outside concessions, so were masked and omitted.

4.2. Influence of flight altitude on oyster table detection

Previous research have suggested that the accuracy of UAV-based photogrammetry-derived products is influenced by flight altitude, with higher altitudes resulting in lower spatial resolution (Anders et al., 2020; Jiang et al., 2020; Liu et al., 2022). In this study, different GSD (Table 1) were achieved by carrying out UAV flights at different altitudes (12, 30, 50, and 120 m) ranging from 0.83 cm per pixel at 12 m to 8.44 cm per pixel at 120 m for the multispectral orthomosaic. At the lower spatial resolution of the 120 m flight only larger features can be identified (Fig. 3), resulting in fewer tie points in the final point cloud during processing. Regardless, the method worked well for the detection of oyster tables for all the flight altitudes tested, although the processing times were not the same in each of the cases. Interestingly, coarser resolutions, which took significantly less processing time, were not outperformed by finer resolutions for oyster table detection. Higher altitude flights can cover larger areas, offering the possibility to map oyster concessions for the whole bay. This reflects the robustness of SfM photogrammetry in using different quality images to reconstruct intertidal environments with relatively good fidelity. For this reason, this GIS-based analytical tool could be used with data obtained at 120 m (maximal authorised flight height) to detect and delineate oyster table footprints for the *ca.* 1700 concessions of Bourgneuf Bay, which cover a surface of around 700 ha. These data obtained at 120 m can provide valuable information when compared with the shellfish cadaster of the Maritime Affairs administration (Fig. 9). Each concession is identified by a polygon and a simple visual examination informs whether they are exploited, unexploited, or if oyster tables have been set up outside the concession area. Within each concession, it is possible to identify double rows of oyster tables in compliance with the SPD (Fig. 9 bottom). This administrative document also indicates that each double row must be separated from the neighboring double rows by a minimal distance of 3 m, which can be easily verified with any GIS software. Additional regulations from this SPD, such as the table height would require a higher spatial resolution as discussed further. Yet, the information on oyster table surface area obtained at 120 m, could be used in conjunction with an *in situ* sampling strategy of measuring oyster bag weights (Cognie et al., 2006) to obtain an estimation of the standing stock of cultivated oysters. This information is crucial to assess the carrying capacity of a shellfish ecosystem (Dame and Prins, 1998) and has not been available in Bourgneuf Bay for more than 20 years.

4.3. Oyster bag mesh size detection

As previously discussed, spatial resolution plays an important role in recognising small targets. On the French Atlantic coast, oysters are cultivated above the ground on trestle tables, placed in plastic bags with different mesh sizes, specifically adapted to the changing size of oysters during the cultivation cycle. The smallest oyster size grown in plastic

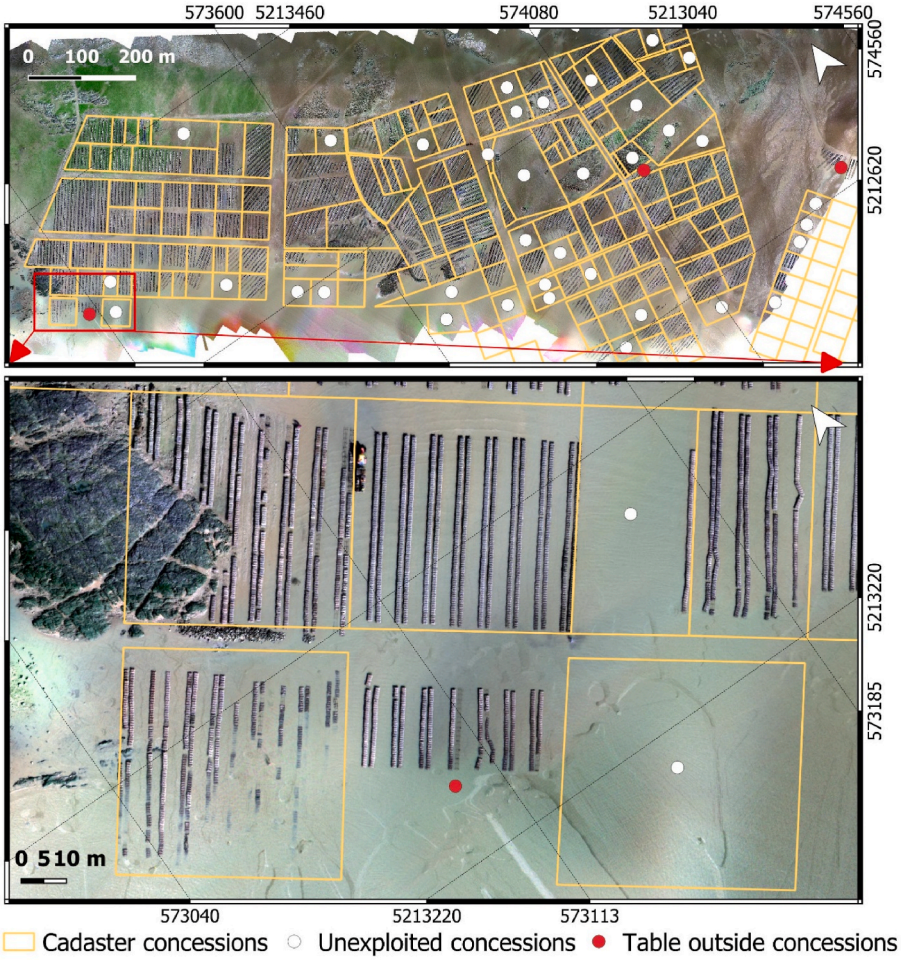

Fig. 9. Shellfish cadaster identifying oyster concessions at "La Bernerie" oyster-farming area, with red dots indicating oyster tables set up outside concessions and white dots indicating unexploited concessions. Below, a zoomed area shows oyster tables organized in paired rows within each concession. (For interpretation of the references to color in this figure legend, the reader is referred to the Web version of this article.)

bags corresponds to the so-called T6 produced by hatcheries: oysters retained by a 6 mm sieve. For these young oysters called spat, 4 mm mesh size bags are used. The largest oysters obtained at the end of the cultivation cycle of 3–4 years are placed in 14 mm mesh-size bags. Between these two mesh sizes, oyster farmers can also use 7 or 9 mm mesh size bags. Identification of the oyster-bag mesh size would allow the distinction of different cohorts with a minimum threshold of discrimination being between spat (4 mm mesh size) and adults (>9 mm mesh size). This information could be useful to obtain a more accurate estimation of the standing stock by applying the respective average biomass estimated for oyster bags used to grow spat and adults respectively. The distinction of cohorts can also be used to assess population demographics (Mann et al., 2009), and to obtain more realistic growth and production scenarios for the management of shellfish ecosystems using modelling approaches (Cugier et al., 2022). In this study, the SVM technique was applied to millimeter-scale spatial resolution UAV data (8.2 mm/px at 12 m flight altitude) in order to distinguish different oyster-bag mesh sizes. Although results generally proved accurate (97.99% OA and 0.95 Kappa coefficient), small misclassification errors also appeared when separating the spectral classes corresponding to the different mesh sizes. These errors are associated with the spectral similarity between the different plastic bags. The mesh size dictates how much can be seen inside the bags and the oyster shells. However, other factors than mesh size can influence the spectral response of an oyster bag. More specifically, each oyster table pixel is composed of optical mixtures combining the spectral responses of the plastic itself, the shell mineralogy, the presence of sediment deposits, the presence of macroalgae and of several epibionts such as cirripeds (Le Bris et al., 2016). At the very high spatial resolution of a 12 m flight (0.83 cm), the producer accuracy for the 4 mm mesh size was 72%, which means that approximately one-quarter of these mesh bags were not correctly identified by the SVM algorithm. Although in general terms the method worked well to classify the different classes for all tested flight heights (with high OA and Kappa coefficients), there was a decrease in the precision of the mesh bags detection with the decrease in spatial resolution, especially in the producer accuracy for the 4 mm mesh size, from 72% at 12 m to 53.85% at 50 m (see Supplementary Material). Thus, based on this, alongside the spectral variability and complexity observed in the field, we concluded that the identification and mapping of oyster-bag mesh sizes could not be achieved at 120 m. It is possible at the operational flight altitude of 50 m (*ie.* that can cover larger areas than 12 and 30 m) but the detection of 4 mm mesh size should be improved with more training data.

4.4. Oyster table height estimation

The SPD stipulates that the oyster table height should be 1 m and no less than 50 cm. Intertidal oyster aquaculture on the French Atlantic coast is often located on soft-bottom sediment and the tables tend to sink into the mud, preventing water from circulating below the tables. Furthermore, table height influences the interaction of oysters with their environment, and is related to growth and mortality. Oyster mortality is markedly altered by host-pathogen interaction (Malek and Byers, 2016; Malek and Byers, 2017), and significant mortalities are related to the Pacific Oyster Mortality Syndrome (POMS) caused by herpesvirus (Lorgeril et al., 2018). Young oysters are notoriously more affected by the herpesvirus 1 than adults, with different mortality risk factors (Gangnery et al., 2019). The tidal exposure time is directly related to the table height, so with higher tables oysters spend more time emersed, being less exposed to OsHV-1 particles showing higher survival (Delisle et al., 2018; De Kantzow et al., 2017). Moreover, longer exposure to higher temperatures during emersion periods at low tide decrease oysters' sensitivity to the virus (Pernet et al., 2019). For farmers and coastal managers, using UAVs could become a fundamental tool to carry out oyster table height control without the need to resort to *in situ* measurements that are labor and time-intensive. This study obtained oyster table height by exploiting topographic data produced by SfM photogrammetry. Modelled heights showed good accuracy when compared with *in situ* data for all flight altitudes tested but the 120 m flight showed less reliable values (Table 4). As expected, the best results were obtained when improving the spatial resolution, although almost equal values were surprisingly obtained when comparing the 12 m and 30 m flights. While the 50 m altitude flight was less consistent across the range of *in situ* oyster table heights, it was still more accurate than the 120 m flight. We therefore suggest that flying at 50 m could be a compromise for the table height estimation, with a larger area being covered.

4.5. Practical recommendations

Traditional methods of monitoring large oyster-farming areas are time-consuming and labor-intensive. Until now, two maritime affairs officers are doing field surveys to check the compliance of each concession with the SPD. With the tidal constraints and the surface to cover this could take several months. In Bourgneuf Bay, the Maritime Affairs administration has recently started to subcontract a commercial UAV company to conduct quicker surveys with RGB drones to check the compliance of oyster concessions with the shellfish cadaster. Our work suggests that more information can be automatically retrieved from very high-resolution multispectral data. Obtaining a high spatial accuracy with a drone equipped with a RTK positioning system would be the best option (Brunier et al., 2022a). If not, as was the case in this study, it is necessary to use a dGPS for the correct georeferencing of UAV data and its validation.

It was possible to retrieve high-resolution 3D models and two-dimensional orthomosaics, obtaining valuable topographic variables such as oyster table height. Despite promising results, there are still some shortcomings of the spectral-based workflow outlined here that could be improved. For example, some small patches of oyster reefs were misclassified as oyster tables. The method was also not adapted to identify oyster tables covered by a small water layer. For future research on intertidal oyster-farming areas, it is recommended that the combination of spectral information and morphological analysis (texture, segmentation, morphometric index from topography …) are combined as has been applied to UAV imagery monitoring of wild oyster reefs. For example, Espriella et al. (2020) successfully performed an Object-Based Image Analysis (GEOBIA) in order to classify mudflat, salt marsh, and oyster reef habitats, obtaining very promising results just employing RGB bands. Espriella and Lecours (2022) also applied a GEOBIA workflow for a multiscale analysis to streamline habitat classifications. Windle et al. (2022) retrieved spectral and structural metrics from SfM photogrammetry with UAV to estimate intertidal wild oyster reef density. In addition, Chand and Bollard (2021) mapped wild oyster reefs with a VNIR sensor mounted on a drone performing a GEOBIA and a SVM classification analysis, showing that it was possible with just a 5 band multispectral sensor. To emulate this work, initially a landform classification using geomorphon analysis (Brunier et al. 2022a, 2022b) was utilised to detect the oyster table footprint. However, high levels of misclassifications were encountered, especially when oyster tables were above water where the DSM reconstruction is highly distorted.

Other important external factors that must be considered when using UAV imagery for shellfish aquaculture monitoring include shadowing, cloud coverage and tidal effects (Joyce et al., 2018). It is important to avoid changes in illumination that can influence the spectral characteristics of oyster tables. Therefore, it is preferable to collect data in clear or completely covered skies. In addition, the solar position can cause shadowing from oyster tables, so it is recommended to plan the UAV surveys close to solar noon and towards the sun azimuth (Windle et al., 2022). In this study, we showed that it was possible to detect oyster table footprints from their spectral characteristics even when there was a water layer below them. However, making the flights coincide with the lowest tide conditions is recommended.

5. Conclusions

In this work, we showed the potential of an UAV-based analytical workflow using machine learning to accurately monitor oyster-farming structures in intertidal areas. The method can enhance traditional *in situ* surveys saving time and money to obtain information on oyster table footprint and table height with an automated process being more efficient than photointerpretation. We tested the method's performance at different spatial resolutions with variable flight heights to help the maritime administration and shellfish farmers optimise the use of UAVs for management purposes. We also demonstrated that spectral data can be used to separate different oyster-bag mesh sizes, although further research combining GEOBIA and multispectral imagery is suggested to reduce misclassification errors. In addition, this tool could be used to understand how oyster aquaculture interacts with the surrounding ecosystem, allowing regulators to deliver actionable information to support smart regulation for aquaculture practices. Eventually, the identification of the oyster mesh-bags for the whole bay could be used with an *ad hoc* sampling strategy of the oyster biomass/total weight per bag to estimate the standing stock of cultivated *Crassostrea gigas*, an essential piece of information to assess the carrying capacity of shellfish ecosystems.

Funding

This research was funded by grants PY20-00244 SAT4ALGAE by Junta de Andalucía. A.R. is supported by grant FPU19/04557 funded by Ministry of Universities of the Spanish Government. H.P. was supported by the Erasmus+: Key Action 1 – Erasmus Mundus Joint Master Degrees (EMJMD) (Grant No. 599111-EPP-1-2018-1-EL-EPPKA1-JMD-MOB) for the EMJMD in Aquaculture, Environment and Society PLUS (ACES+). This work represents a contribution to CSIC Thematic Interdisciplinary Platform PTI TELEDETECT.

CRediT authorship contribution statement

Alejandro Román: Writing – review & editing, Writing – original draft, Software, Methodology, Investigation. **Hermansyah Prasyad:** Writing – review & editing. **Simon Oiry:** Writing – review & editing, Validation, Software, Data curation. **Bede F.R. Davies:** Writing – review & editing, Investigation, Formal analysis, Data curation. **Guillaume Brunier:** Writing – review & editing, Methodology. **Laurent Barillé:** Writing – review & editing, Writing – original draft, Supervision, Investigation, Conceptualization.

Declaration of competing interest

The authors declare that they have no known competing financial interests or personal relationships that could have appeared to influence the work reported in this paper.

Data availability

No data was used for the research described in the article.

Appendix A. Supplementary data

Supplementary data to this article can be found online at https://doi.org/10.1016/j.ecss.2023.108432.

References

Alberg, A.J., Park, J.W., Hager, B.W., Brock, M.V., Diener-West, M., 2004. The use of "overall accuracy" to evaluate the validity of screening or diagnostic tests. J. Gen. Intern. Med. 19 (5), 460–465. https://doi.org/10.1111/j.1525-1497.2004.30091.x.

Anders, N., Smith, M., Suomalainen, J., Cammeraat, E., Valente, J., Keesstra, S., 2020. Impact of flight altitude and cover orientation on Digital Surface Model (DSM) accuracy for flood damage assessment in Murcia (Spain) using a fixed-wing UAV. Earth Sci. Inf. 13, 391–404. https://doi.org/10.1007/s12145-019-00427-7.

Anderson, D., Heiss, A., Sumners, J., 2023. Equatiomatic: Transform Models into LaTeX Equations. https://github.com/datalorax/equatiomatic. (Accessed 11 July 2023).

Bahari, N.I.S., Ahmad, A., Aboobaider, B.M., 2014. Application of support vector machine for classification of multispectral data. IOP Conf. Ser. Earth Environ. Sci. 20 (1), 0–8. https://doi.org/10.1088/1755-1315/20/1/012038.

Barillé, L., Le Bris, A., Goulletquer, P., Thomas, Y., Glize, P., Kane, F., Falconer, L., Guillotreau, P., Trouillet, B., Palmer, S., Gernez, P., 2020. Biological, socio-economic, and administrative opportunities and challenges to moving aquaculture offshore for small French oyster-farming companies. Aquaculture 521, 735045. https://doi.org/10.1016/j.aquaculture.2020.735045.

Bell, T.W., Nidzieko, N.J., Siegel, D.A., Miller, R.J., Cavanaugh, K.C., Nelson, N.B., Reed, D.C., Fedorov, D., Moran, C., Snyder, J.N., Cavanaugh, K.C., Yorke, C.E., Griffith, M., 2020. The utility of satellites and autonomous remote sensing platforms for monitoring offshore aquaculture farms: a case study canopy forming kelps. Front. Mar. Sci. 7, 520223 https://doi.org/10.3389/fmars.2020.520223.

Brunier, G., Oiry, S., Gruet, Y., Dubois, S.F., Barillé, L., 2022a. Topographic analysis of intertidal polychaete reefs (sabellaria alveolata) at a very high spatial resolution. Rem. Sens. 14 (2), 307. https://doi.org/10.3390/rs14020307.

Brunier, G., Oiry, S., Lachaussée, N., Barillé, L., Le Fouest, V., Méléder, V., 2022b. A machine-learning approach to intertidal mudflat mapping combining multispectral reflectance and geomorphology from UAV-based monitoring. Rem. Sens. 14 (22), 5857. https://doi.org/10.3390/rs14225857.

Buestel, D., Ropert, M., Prou, J., Goulletquer, P., 2009. History, status, and future of oyster culture in France. J. Shellfish Res. 28, 813–820. https://doi.org/10.2983/035.028.0410.

Candiago, S., Remondino, F., De Gilgio, M., Dubbini, M., Gattelli, M., 2015. Evaluating multispectral images and vegetation indices for precision farming applications from UAV images. Rem. Sens. 7 (4), 4026–4047. https://doi.org/10.3390/rs70404026.

Chand, S., Bollard, B., 2021. Multispectral low altitude remote sensing of wild oyster reefs. Global Ecol. Conserv. 30, e01810 https://doi.org/10.1016/j.gecco.2021.e01810.

Cognie, B., Haure, J., Barillé, L., 2006. Spatial distribution in a temperate coastal ecosystem of the wild stock of the farmed oyster Crassostrea gigas (Thunberg). Aquaculture 259 (1–4), 249–259. https://doi.org/10.1016/j.aquaculture.2006.05.037.

Conrad, O., Bechtel, B., Bock, M., Dietrich, H., Fisher, E., Gerlitz, L., Wehberg, J., Wichmann, V., Böhner, J., 2015. System for automated geoscientific analyses (SAGA) V. 2.1.4. Geosci. Model Dev. (GMD) 8 (7), 1991–2007, 10. 5194/gmd-8-1991-2015.

Cugier, P., Thoma, Y., Bacher, C., 2022. Ecosystem modelling to assess the impacto f rearing density, environment variability and mortality on oyster production. Aquac. Environ. Interact. 14, 53–70. https://doi.org/10.3354/aei00428.

Dame, R.F., Prins, T.C., 1998. Bivalve carrying capacity in coastal ecosystems. Aquat. Ecol. 31, 409–421. https://doi.org/10.1023/A:1009997011583.

Dean, A., Salim, A., Kapetsky, J.M., Aguilar-Manjarrez, J., Jenness, J., 2013. Remote sensing for the sustainable development of offshore mariculture. In: A Global Assessment of Offshore Mariculture Potential from a Spatial Perspective. FAO Fisheries and Aquaculture Technical Paper N. 549 Rome, FAO, pp. 123–181.

Decottignies, P., Beninger, P.G., Rincé, Y., Robins, R.J., Riera, P., 2007. Exploitation of natural food sources by two sympatric, invasive suspension-feeders: Crassostrea gigas and Crepidula fornicata. MEPS 334, 179–192. https://doi.org/10.3354/meps334179.

Delisle, L., Petton, B., Burguin, J.F., Morga, B., Corporeau, C., Pernet, F., 2018. Temperature modulate disease susceptibility of the Pacific oyster Crassostrea gigas and virulence of the Ostreid herpesvirus type 1. Fish Shellfish Immunol. 80, 71–79. https://doi.org/10.1016/j.fsi.2018.05.056.

De Kantzow, M.C., Hick, P.M., Dhand, N.K., Whittington, R.J., 2017. Risk factors for mortality during the first occurrence of pacific oyster mortality Syndrome due to ostreid herpesvirus-1 in tasmania, 2016. Aquaculture 468, 328–336. https://doi.org/10.1016/j.aquaculture.2016.10.025.

Echappé, C., Gernez, P., Méléder, V., Jesus, B., Cognie, B., Decottignies, P., Sabbe, K., Barillé, L., 2018. Satellite remote sensing reveals a positive impact of living oyster reefs on microalgal biofilm development. Biogeosciences 15, 905. https://doi.org/10.5194/bg-15-905-2018, 018.

Espriella, M.C., Lecours, V., 2022. Optimizing the scale of observation for intertidal habitat classification through multiscale analysis. Drones 6, 140. https://doi.org/10.3390/drones6060140.

Espriella, M.C., Lecours, V., Frederick, P.C., Camp, E.V., Wilkinson, B., 2020. Quantifying intertidal habitat relative coverage in a Florida estuary using UAS imagery and GEOBIA. Rem. Sens. 12, 677. https://doi.org/10.3390/rs12040677.

FAO, 2023. Global Aquaculture Production. Fisheries and Aquaculture Division [online]. Rome. https://www.fao.org/fishery/en/collection/aquaculture?lang=en. (Accessed 18 January 2023).

FAO, 2022. The state of world fisheries and aquaculture 2020. In: Sustainability in Action. FAO, Rome. https://doi.org/10.4060/cc0461en. (Accessed 18 January 2023).

FAO, 2011. Crassostrea gigas (Thunberg, 1793). FAO Aquat. Species Inf. Progr. 86, 271–278.

Gangnery, A., Normand, J., Duval, C., Cugier, P., Grangeré, K., Petton, B., Petton, S., Orvain, F., Pernet, F., 2019. Connectivities with shellfish farms and channel rivers are associated with mortality risk in oysters. Aquac. Environ. Interact. 11, 493–506. https://doi.org/10.3354/aei00327.

Gernez, P., Palmer, S.C.J., Thomas, Y., Forster, R., 2021. Editorial: remote sensing for aquaculture. Front. Mar. Sci. 7, 2020–2022. https://doi.org/10.3354/aei00115.

Gernez, P., Doraxan, D., Barillé, L., 2017. Shellfissh aquaculture from Space: potential of Sentinel 2 to monitor tide-driven changes in turbidity, chlorophyll concentration and oyster physiological response at the scale of an oyster farm. Front. Mar. Sci. 4, 137. https://doi.org/10.3389/fmars.2017.00137.

Gernez, P., Barillé, L., Lerouxel, A., Mazeran, C., Lucas, A., Doxaran, D., 2014. Remote sensing of suspended particulate matter in turbid oyster-farming ecosystems. J. Geophys. Res. Oceans 119 (10), 7277–7294. https://doi.org/10.1002/2014JC010055.

Guillotreau, P., Le Bihan, V., Pardo, S., 2018. Mass mortality of farmed oyster in France: bad responses and good results. In: Guillotreau, P., Bundy, A., Perry, R.I. (Eds.), Global Change in Marine Systems, Integrating Societal and Governing Responses. Routledge Studies in Environment, Culture and Society (RSECS) Series Routledge, pp. 54–64, 9781315163765.

Harris, J., 2008. Pacific Oyster, Crassostrea gigas (Thunberg, 1793). Aquatic Invasion Ecology, pp. 1–12.

Hedley, C., Huntington, T., 2009. Regulatory and Legal Constraints for European Aquaculture. European Parliament, pp. 1–102.

Jiang, B., Boss, E., Kiffney, T., Hesketh, G., Bourdin, G., Fan, D., Brady, D.C., 2022. Oyster aquaculture site selection using high-resolution remote sensing: a case study in the Gulf of Maine, United States. Front. Mar. Sci. 9, 802438 https://doi.org/10.3389/fmars.2022.802438.

Jiang, R., Wang, P., Xu, Y., Zhou, Z., Luo, X., Lan, Y., Zhao, G., Sanchez-Azofeifa, A., Laakso, K., 2020. Assessing the operation parameters of a low-altitude UAV for the collection of NDVI values over a paddy rice field. Rem. Sens. 12, 1850. https://doi.org/10.3390/rs12111850.

Joyce, K.E., Duce, S., Leahy, S.M., Leon, J., Maier, S.W., 2018. Principles and practice of acquiring drone-based image data in marine environments. Mar. Freshw. Res. 70 (7), 952–963. https://doi.org/10.1071/MF17380.

Kay, M., Patel, S.N., Kientz, J.A., 2017. How do you know if 85% accuracy is good enough for your application? GetMobile: Mobile Comput. Commun. 21 (2), 5–8. https://doi.org/10.1145/3131214.3131216.

Kervella, Y., Germain, G., Gaurier, B., Facq, J.V., Cayocca, F., Lesueur, P., 2010. Experimental study of the near-field impact of an oyster table on the flow. Eur. J. Mech. B Fluid 29, 32–42. https://doi.org/10.1016/j.euromechflu.2009.09.002.

Le Bris, A., Rosa, P., Lerouxel, A., Cognie, B., Gernez, P., Launeau, P., Robin, M., Barillé, L., 2016. Hyperspectral remote sensing of wild oyster reefs. Estuar. Coast Shelf Sci. 172, 1–12. https://doi.org/10.1016/j.ecss.2016.01.039.

Liu, Y., Han, K., Rasdorf, W., 2022. Assessment and prediction of impact of flight configuration factor son UAS-based photogrammetric survey accuracy. Rem. Sens. 14, 4119. https://doi.org/10.3390/rs14164119.

Lorgeril, L., Lucasson, A., Petton, B., Toulza, E., Montagnani, C., Clerissi, C., Vidal-Dupiol, J., Chaparro, C., Galinier, R., Escoubas, J., Haffner, P., Dégremont, L., Charrière, G.M., Lafont, M., Delort, A., Vergnes, A., Chiarello, M., Faury, N., Rubio, T., Leroy, M.A., Pérignon, A., Régler, D., Morga, B., Alunno-Bruscia, M., Boudry, P., Le Roux, F., Destoumieux-Garzón, D., Gueguen, Y., Mitta, G., 2018. Immune-suppression by OsHV-1 viral infection causes fatal bacteraemia in Pacific oysters. Nat. Commun. 9, 4215. https://doi.org/10.1038/s41467-018-06659-3.

Malek, J.C., Byers, J.E., 2016. Effects of air-exposure gradients on spatial infection patterns of Perkinsus marinus in the Eastern oyster Crassostrea virginica. Dis. Aquat. Org. 118, 139–151. https://doi.org/10.3354/dao02964.

Malek, J.C., Byers, J.E., 2017. The effects of tidal elevation on parasite heterogeneity and co-infection in the eastern oyster, Crassostrea gigas. Aquaculture 412–413, 202–214. https://doi.org/10.1016/j.jembe.2017.05.004.

Mallet, C., David, N., 2016. 7 – digital terrain models derived from airborne LiDAR data. Opt. Rem. Sens. Land Surface 299–319. https://doi.org/10.1016/B978-1-78548-102-4.50007-7.

Mann, R.L., Southworth, M., Harding, J.M., Wesson, J.A., 2009. Population studies of the native eastern oyster, Crassostrea virginica, (Gmelin, 1791) in the james river, Virginia, USA. J. Shellfish Res. 28 (2), 193–220. https://doi.org/10.2983/035.028.0203.

Martínez-García, M.F., Ruesink, J.L., Grijalva-Chon, J.M., Lodeiros, C., Arreola-Lizárraga, J.A., Re-Vega, E., Varela-Romero, A., Chávez-Villalba, J., 2021. Socioecological factors related to aquaculture introductions and production of Pacific oysters (*Crassostrea gigas*) worldwide. Rev. Aquacult. 14, 613–629. https://doi.org/10.1111/raq.12615.

Miossec, L., Le Deuff, R.M., Goulletquer, P., 2009. Alien species alert: Crassostrea gigas (pacific oyster). ICES (Int. Counc. Explor. Sea) Coop. Res. Rep. 299, 1–42, 978–87–7482–069–7.

Miranda, V., Pina, P., Heleno, S., Vieira, G., Mora, C., Schaefer, C.E.G.R., 2020. Monitoring recent changes of vegetation in fildes peninsula (king George island, Antarctica) through satellite imagery guided by UAV surveys. Sci. Total Environ. 704, 135295 https://doi.org/10.1016/j.scitotenv.2019.135295.

Newell, R.I.E., 2004. Ecosystem influences of natural and cultivated populations of suspension-feeding bivalve molluscs: a review. J. Shellfish Res. 23 (1), 51–61.

Oloffson, P., Foody, G.M., Herold, M., Stehman, S.V., Woodcock, C.E., Wulder, M.A., 2014. Good practices for estimating area and assessing accuracy of land change. Remote Sens. Environ. 148, 42–57. https://doi.org/10.1016/j.rse.2014.02.015.

Oullette, W., Getinet, W., 2016. Remote sensing for marine spatial planning and integrated coastal areas management: achievements, challenges, opportunities and future prospects. Remote Sens. Appl.: Soc. Environ. 4, 138–157. https://doi.org/10.1016/j.rsase.2016.07.003.

Palmer, S.C.J., Gernez, P.M., Thomas, Y., Simis, S., Miller, P.I., Glize, P., Barillé, L., 2020. Remote sensing-driven pacific oyster (*Crassostrea gigas*) growth modeling to inform offshore aquaculture site selection. Front. Mar. Sci. 6, 1–19. https://doi.org/10.3389/fmars.2019.00802.

Pernet, F., Gachelin, S., Stanisière, J., Petton, B., Fleury, E., Mazurié, J., 2019. Farmer monitoring reveals the effect of tidal height on mortality risk of oysters during a herpesvirus outbreak. ICES (Int. Counc. Explor. Sea) J. Mar. Sci. 76 (6), 1816–1824. https://doi.org/10.1093/icesjms/fsz074.

Pincinato, R.B.M., Asche, F., Bleie, H., Skrudland, A., Stormoen, M., 2021. Factors influencing production loss in salmonid farming. Aquaculture 532, 736034. https://doi.org/10.1016/j.aquaculture.2020.736034.

R Core Team, 2022. A Language and Environment for Statistical Computing. R Foundation for Statistical Computing, Vienna, Austria. https://www.R-project.org/. (Accessed 19 January 2023).

Román, A., Tovar-Sánchez, A., Olivé, I., Navarro, G., 2021. Using a UAV-mounted multispectral camera for the monitoring of marine macrophytes. Front. Mar. Sci. 8, 722698 https://doi.org/10.3389/fmars.2021.722698.

Saitoh, S.I., Mugo, R., Radiarta, I.N., Asaga, S., Takahashi, F., Hirawake, T., Ishikawa, Y., Awaji, T., In, T., Shima, S., 2011. Some operational uses of satellite remote sensing and marine GIS for sustainable fisheries and aquaculture. ICES (Int. Counc. Explor. Sea) J. Mar. Sci. 68 (4), 687–695. https://doi.org/10.1093/icesjms/fsq190.

Snyder, J., Boss, E., Weatherbee, R., Thomas, A.C., Brady, D., Newell, C., 2017. Oyster aquaculture site selection using Landsat-8-derived sea surface temperatura, turbidity and chlorophyll a. Front. Mar. Sci. 4, 190. https://doi.org/10.3389/fmars.2017.00190.

Vapnick, V., 1995. The Nature of Statisstical Learning Theory. Springer-Verlag, New York, NY.

Wickham, H., 2022. Tidyversse: easily install and load the tidyverse. https://CRAN.R-project.org/package=tidyverse. (Accessed 19 January 2023).

Windle, A.E., Puckett, B., Huebert, K.B., Knorek, Z., Johnston, D.W., Ridge, J.T., 2022. Estimation of intertidal oyster reef density using spectral and structural characteristics derived from unoccupied aircraft systems and structure from motion photogrammetry. Rem. Sens. 14, 2163. https://doi.org/10.3390/rs14092163.

Windle, A.E., Poulin, S.K., Johnston, D.W., Ridge, J.T., 2019. Rapid and accurate monitoring of intertidal oyster reef habitat using unoccupied aircraft systems and structure from motion. Rem. Sens. 11, 2394. https://doi.org/10.3390/rs11202394.